Design of Machines and Structures, Vol. 9, No. 1 (2019), pp. 29–47.
https://doi.org/10.32972/dms.2019.004

COMPUTATIONAL FLUID DYNAMIC SIMULATION OF LAMINAR FLOW OVER A FLAT PLATE

MOHAMAD MEHI ALDDIN KLAZLY–GABRIELLA BOGNÁR

University of Miskolc, Department of Machine and Product Design
3515 Miskolc-Egyetemváros
machhkme@uni-miskolc.hu

Abstract: The aim of this work is to apply CFD simulation on airflow over a flat plate to study the problem of hydrodynamic and thermal boundary layer and to analyse the effect of the length of the plate. The simulation ANSYS Fluent R18.1 has been applied to solve the governing equations of the flow. The simulation results have been verified by comparing the numerical solution with the analytical solution. The effect of changing the length of the plate is investigated while the other quantities were considered constant such as the free stream velocity, density, viscosity and temperature. The result showed excellent agreement between the numerical solution and analytical solution with maximum error of less than 6.19%. It is obtained that as the plate length increases the maximum value of the velocity contour, the Nusselt number, the wall shear stress, the skin friction coefficient and drag coefficient decreases.

Keywords: *CFD, boundary layer, numerical method, skin friction coefficient, heat transfer coefficient*

1. INTRODUCTION

Simulations of fluid mechanics flow using Computational Fluid Dynamic (CFD) are the key to solve many problems in mechanical engineering application. It has been used to understand fluid flow behaviour, which is essential in designing and developing any engineering application. One of the most common problems is flow behaviour in the boundary layer. Our aim is to consider hydrodynamic and thermal boundary layer problems of incompressible flow over a horizontal flat plate. The solution of the 2D laminar boundary layer of an incompressible flow formed on a semi-infinite plate has been introduced by Blasius using the similarity solution in 1908 [1], then, in 1938, Howarth gave a new solution using the Runge–Kutta method for analysing the flow over the flat plate [2]. Other methods in 1994, Abu-Sitta investigated and established the existence of the solution [3]. Moreover, the finite difference methodology was employed to get the numerical solution of the Falkner-Skan equation by Asaithambi [4], [5], [6]. Recently, the Blasius equation has been studied by applying different types of numerical and analytical techniques, for example using Adomain Decomposition Method (ADM) [7], [8], [9], and using Homotopy Perturbation Method (HPM) [10], [11]. Our work is motivated by the desire to apply the CFD simulation of flow over a flat plate and to obtain the numerical solution for the velocity and temperature distribution and to analyse at the wall the effect of plate's length on different variables.

2. MATHEMATICAL FORMULAS

Let us consider the problem of a two-dimensional flow of steady, Newtonian and incompressible fluid. The gravity is neglected, and all the fluid properties are assumed to be constant. When fluid flows over the impermeable plate, a thin boundary layer will develop

near the plate surface because of the no-slip condition. The viscous effect on the flow inside this layer is very important and has to be studied well, while region outside this hydrodynamic layer can be treated as an inviscid flow.

Laminar boundary layer equations:

We consider the problem of hydrodynamic and thermal boundary layer over a flat plate in a stream of air at temperature $T_\infty = 300$ K far from the plate and moving with uniform velocity $U_\infty = 1.5\ \mathrm{m/s}$. The temperature of the plate is $T_w = 400$ K. The governing equations, continuity, momentum and energy equations can be written as follows:

$$\frac{\partial u}{\partial x} + \frac{\partial v}{\partial y} = 0, \tag{1}$$

$$u\frac{\partial u}{\partial x} + v\frac{\partial u}{\partial y} = \upsilon\frac{\partial^2 u}{\partial y^2}, \tag{2}$$

$$u\frac{\partial T}{\partial x} + v\frac{\partial T}{\partial y} = \alpha\frac{\partial^2 T}{\partial y^2}, \tag{3}$$

where:
u and v: components of the velocity in *x* and *y* directions, respectively,
U_∞: free stream velocity,
T_∞: temperature of free stream,
α: thermal diffusivity of the fluid,
υ: kinematic viscosity of the fluid.

The fluid flow *Equations (1)–(3)* are subjected to the boundary conditions as follows:

at the plate as: $y = 0, \quad u = 0, \quad v = 0, \quad T = T_w,$ (4)

and far from the plate as $y \to \infty$, $u = U_\infty, \quad T = T_\infty$. (5)

The system (1)–(3) can be solved using similarity method applying stream function $\psi = \sqrt{2\upsilon x U_\infty}\, f(\eta)$, where f is the non-dimensional stream function and $\eta = y\sqrt{\frac{U_\infty}{2\upsilon x}}$ is the similarity variable. Then system (1)–(2) can be transformed into the well-known Blasius equation with $u = \frac{\partial \psi}{\partial y}$ and $v = -\frac{\partial \psi}{\partial x}$.

$$f''' + ff' = 0, \tag{6}$$

with boundary conditions

$$f(0) = 0, \quad f'(0) = 0, \quad f'(\eta_\infty) = 1. \tag{7}$$

For the energy *Equation (3)*, the similarity transformation $\emptyset = \frac{T-T_\infty}{T_w-T_\infty}$ is used. Then the *Equation (3)* is written as

$$\frac{\alpha}{\upsilon}\emptyset'' + \emptyset' f = 0, \tag{8}$$

with boundary conditions

$$\emptyset(0) = 1, \qquad \emptyset(\eta_\infty) = 0.$$

Applying $\mathrm{Pr} = \frac{\alpha}{\upsilon}$ we have from (8)

$$\emptyset'' + Pr\ \emptyset' f = 0$$

The temperature and velocity components with similarity function f and $\emptyset$ are as follows $T = \emptyset(T_w - T_\infty) + T_\infty, \quad u = U_\infty f'(\eta)$ and $v = \sqrt{\frac{\upsilon U_\infty}{2x}}(\eta f' - f)$.

The analytical solution for the skin friction coefficient (C_f), the average Nusselt number ($\bar{N}_L$), average convection heat transfer coefficient ($\bar{h}$) and local Nusselt number (Nu_x) can be given by the expressions below [12]:

$$C_f = \frac{0.664}{\sqrt{\mathrm{Re}_x}}, \tag{9}$$

$$\overline{\mathrm{Nu}}_L = 0.664\,\frac{\rho U_\infty L}{\mu}, \tag{10}$$

$$\bar{h} = \frac{\bar{N}_L k}{L}, \tag{11}$$

$$\mathrm{Nu}_x = 0.332\ \mathrm{Re}_x^{\frac{1}{2}}\ \mathrm{Pr}^{\frac{1}{3}}, \tag{12}$$

$$C_D = \frac{F_x}{\frac{1}{2}\rho U_\infty^2 L}, \tag{13}$$

$$\mathrm{Re} = \frac{\rho U_\infty L}{\mu}, \tag{14}$$

$$\mathrm{Pr} = \frac{\alpha}{\upsilon}. \tag{15}$$

where:
C_f: skin friction coefficient,
C_D: drag coefficient,
Re: Reynold's number for the plate,
Re_x: Reynold's number at distance *x*,

ρ: density of the fluid,
μ: dynamic viscosity of the fluid,
L: length of the plate,
$\overline{h}$: average convection heat transfer coefficient,
$\overline{\mathrm{Nu}}_L$: average Nusselt number,
Nu_x: local Nusselt number,
Pr: Prandtl number,
k: thermal conductivity of the fluid,
F_x: horizontal force acting on the plate.

3. COMPUTATIONAL FLUID DYNAMICS METHOD (CFD)

Computational fluid dynamics is used for solving and analysing fluid flow problems numerically. The procedure of applying the CFD as the follow:

3.1. Creating the geometry

The first step is to model the problem and to create the geometry. The geometry of the model has created using Design Modeler. The flow configuration is represented in *Figure 1*. The boundary BC is defined as surface wall, AD defined as symmetry, and the boundaries AB and CD are defined as inlet and outlet, respectively.

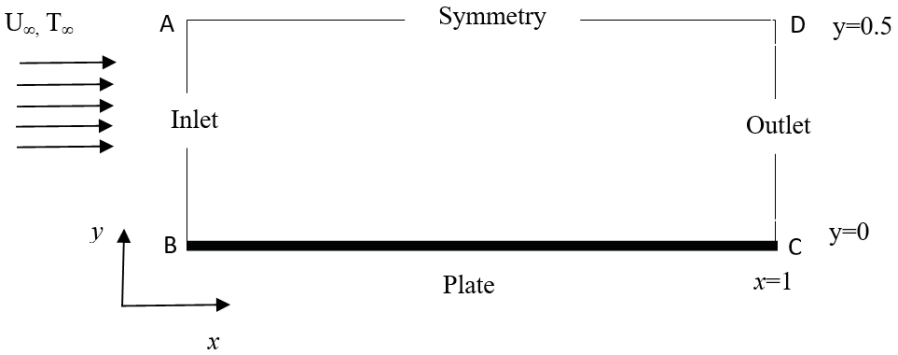


Figure 1. The flow configuration

3.2. Creating the mesh and name selection

Meshing is the second step of CFD simulation. For analysing the fluid flow, the flow domain splits into finer subdomains, for two-dimensional geometry it can be made up for quadrilaterals or triangles. Then, the governing equations are discretized and solved for these small subdomains. For our model the fluent mesh is used to create the meshing. The inlet and outlet have been divided by the number of division type with 100 divisions, the behaviour was set to hard with bias factor 100 to increase the number of subdomains near to the plate which is the important area and consequently the preciseness can increase. The sides symmetry and plate are divided using the same method with 60 divisions. *Figure 2* shows the result of mesh generation.

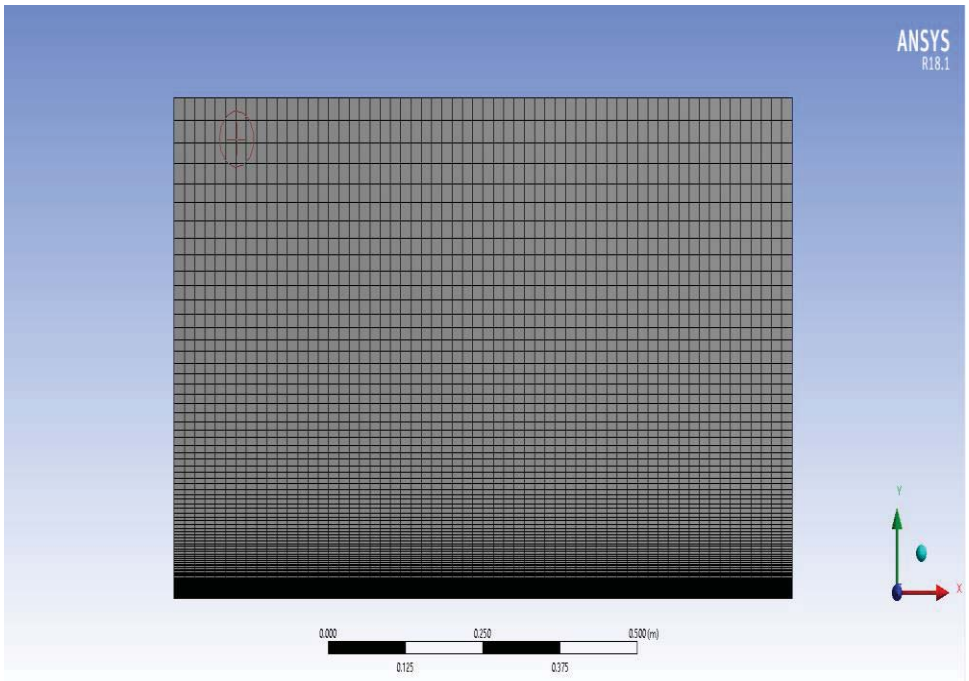


Figure 2. Meshing

3.3. Setting up the physical values

Here the flow and thermal variables (boundary conditions) on our physical model are specified. The boundary conditions and the fluid properties that have been used are the following according to the ANSYS FLUENT code. The boundary AB is defined as velocity inlet where the horizontal velocity is constant, and the vertical velocity is zero. The boundary CD is defined as pressure outlet, where the static pressure is placed equal to ambient pressure and all other flow quantities are extrapolated from the interior. The plate BC is defined as wall, where both the horizontal and vertical velocities are zero, and the far field AD is considered as symmetry where the velocity gradients in the vertical direction are forced to be zero. *Table 1* contains the physical properties of the fluid and flow.

Table 1
The physical properties

Name	Fluid properties	Value
density	ρ	1.225
dynamic viscosity	μ	1.7894×10^{-5}
length	L	1
ambient fluid velocity	U_∞	1.5
ambient fluid temperature	T_∞	300
wall temperature	T_w	400
thermal conductivity of the fluid	k	0.0242
Prandtl number	Pr	0.744176

3.4. Solution

The next step is to obtain the numerical solution, where the Navier–Stokes equations with the energy equation are solved. Laminar solver was used with second-order upwind scheme in the discretization of the set of governing equations. Double precision accuracy was used, and the solution was monitored using a residual monitor with convergence criteria 10^{-8}.

4. RESULT AND DISCUSSION

The results of the hydrodynamic and thermal boundary layers will be presented and discussed.

4.1. Hydrodynamic boundary layer

Figures 3 and *4* introduce the velocity distribution for the flow over the plate. The velocity at the plate is the lowest and it increases till became uniform in the inviscid area, which located above the boundary layer edge. The velocity vectors along with the plate *(*see *Figure 4)* shows that the velocity of fluid particles at the plate is zero due to the no-slip condition and this occurred due to the viscous effect, where the fluid particles stuck to the plate. The highest pressure was located near the leading edge and became lower as we go close to the outlet as can be seen in *Figure 5*.

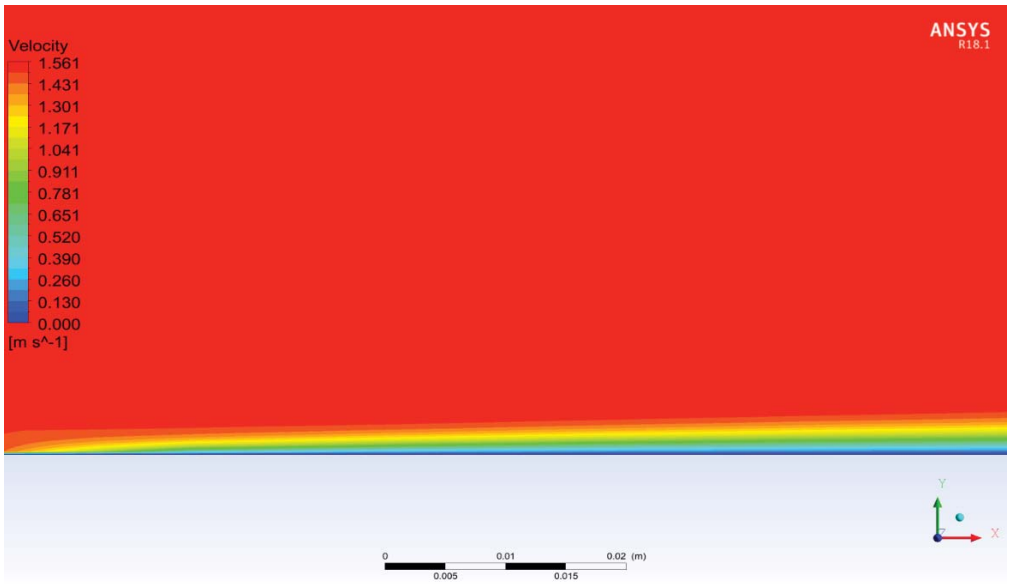


Figure 3. Velocity contour

Figures 6 and *7* show the comparison of velocities at three different locations at $\frac{X}{L} = \frac{1}{3}, \frac{X}{L} = \frac{2}{3}$ and $\frac{X}{L} = 1$. The maximum value of the velocity decrease from the left side to the right side far from the inlet, the maximum value of the velocity was 1.561 m/s *(*see *Figure 3)*.

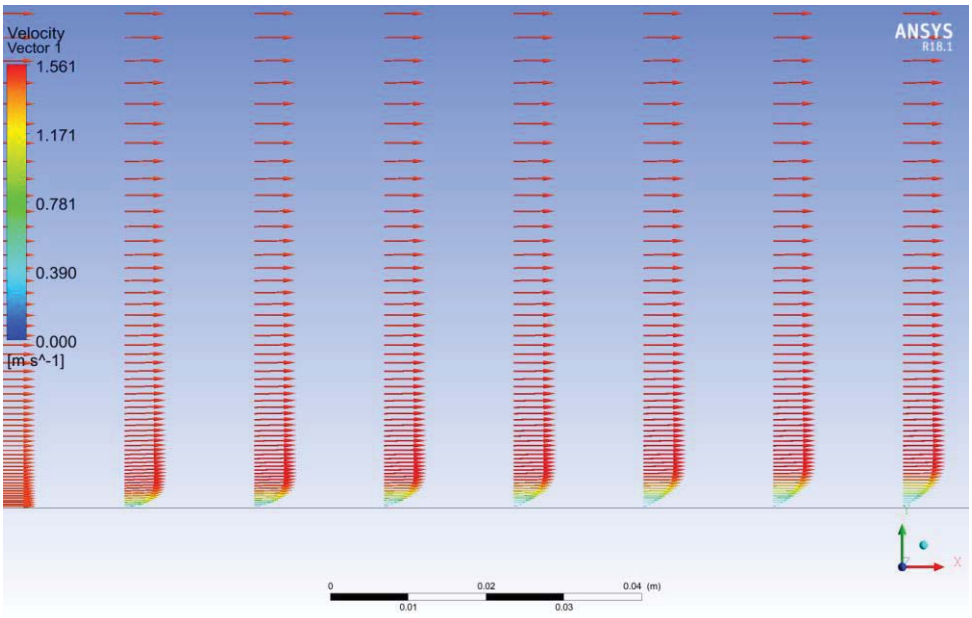


Figure 4. Velocity direction

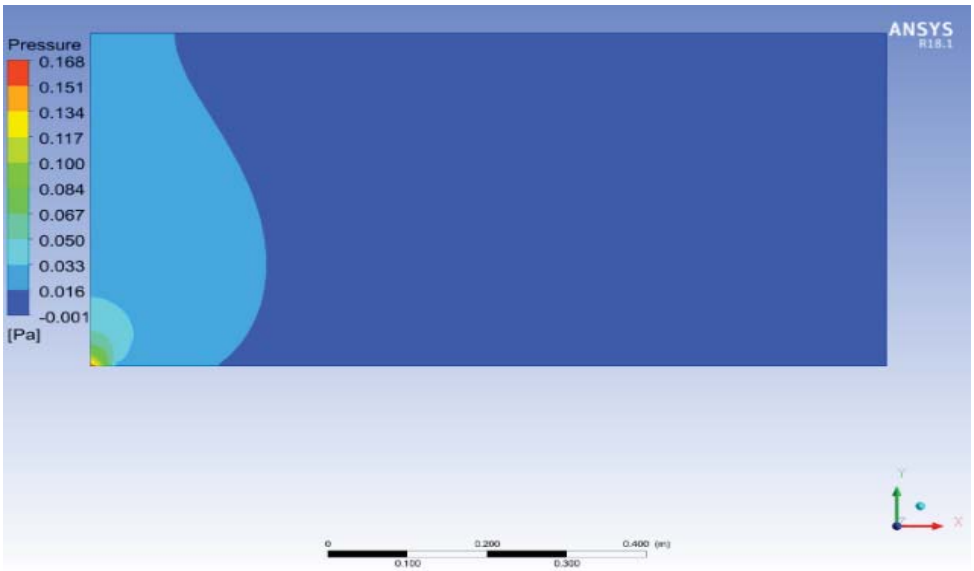


Figure 5. Pressure contour

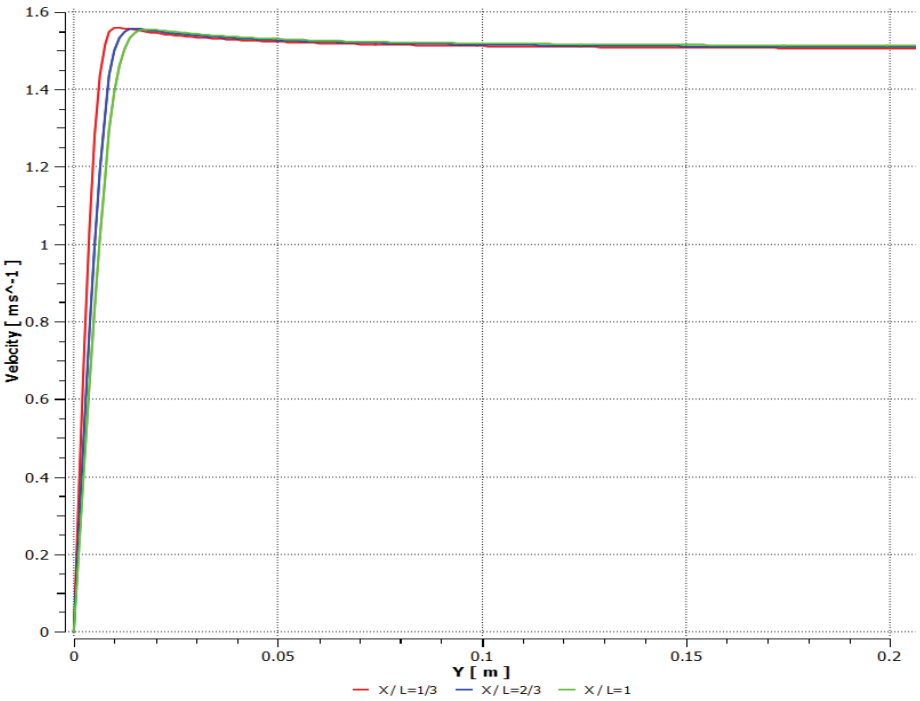


Figure 6. Velocity at different distances from the leading edge

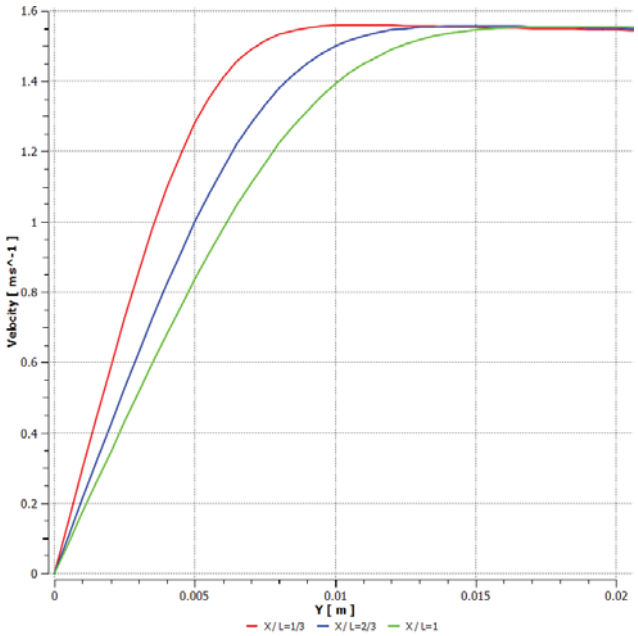


Figure 7. Velocity distributions at different distances from the leading edge

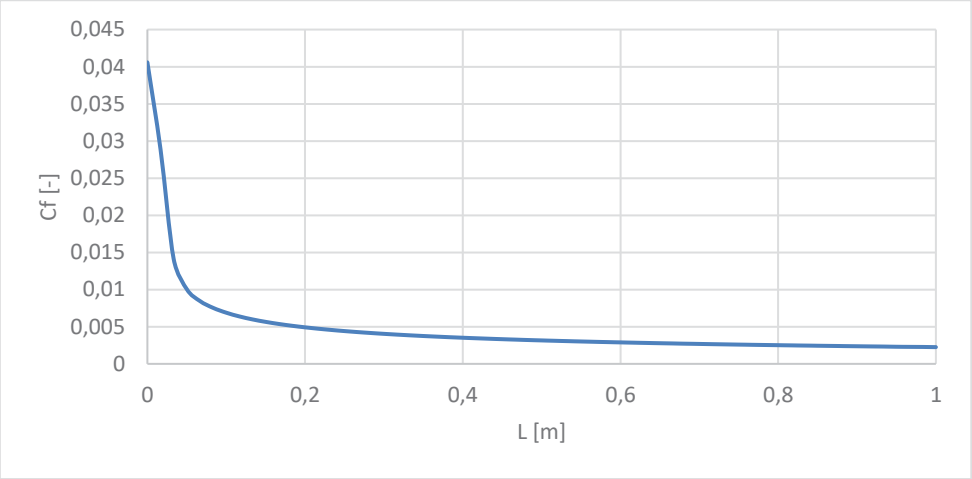


Figure 8. Skin friction coefficient

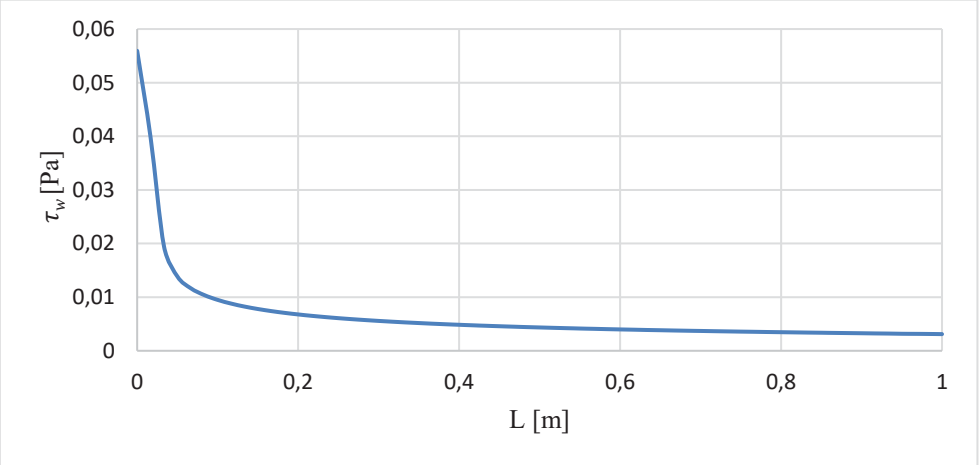


Figure 9. Wall shear stress

The skin friction coefficient is plotted on Fig. 8 along with the length of the plate, and value at the leading edge is 0.0405876 Pa. The wall shear stress is plotted on *Figure 9*. The value of shear stress at the leading edge of the plate was 0.0559349 Pa.

4.2. Thermal boundary layer

The result of the temperature distribution along the plate is presented in *Figure 10*. The temperature at the plate is the highest and it decreases till became uniform and equal to the free stream temperature which was 300 K. The variation of temperature due to the heat convention between the plate and the fluid mainly depends on the value of the thermal conductivity of the fluid.

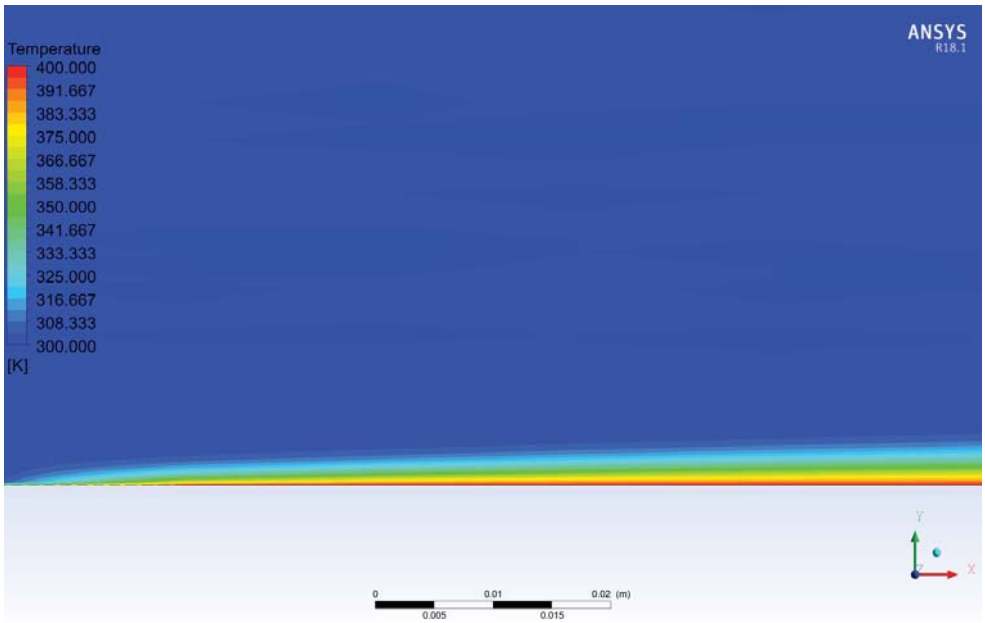


Figure 10. Temperature distribution

Figure 11 shows the total surface heat flux along with the plate and the surface heat transfer coefficient along the plate on *Figure 12*.

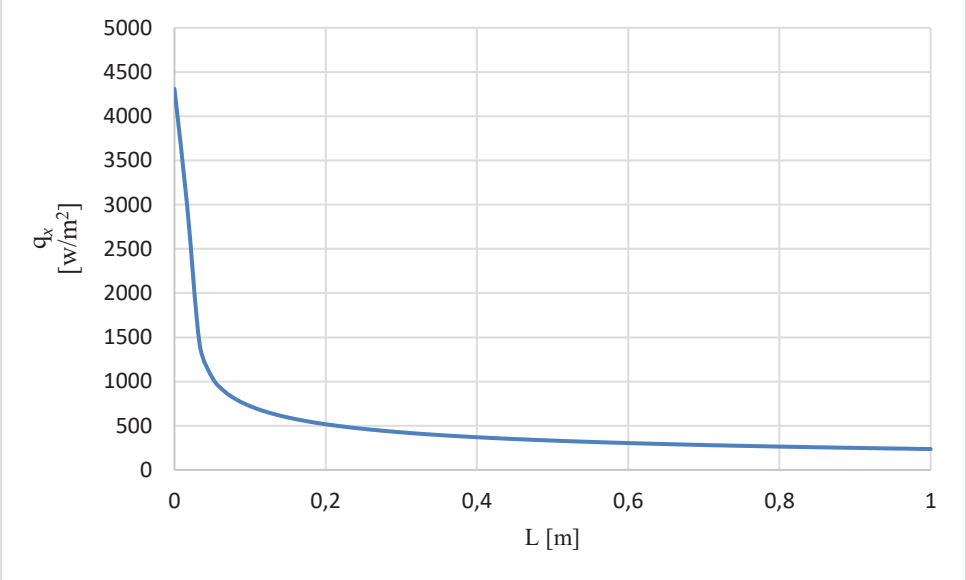


Figure 11. The surface heat flux along the plate

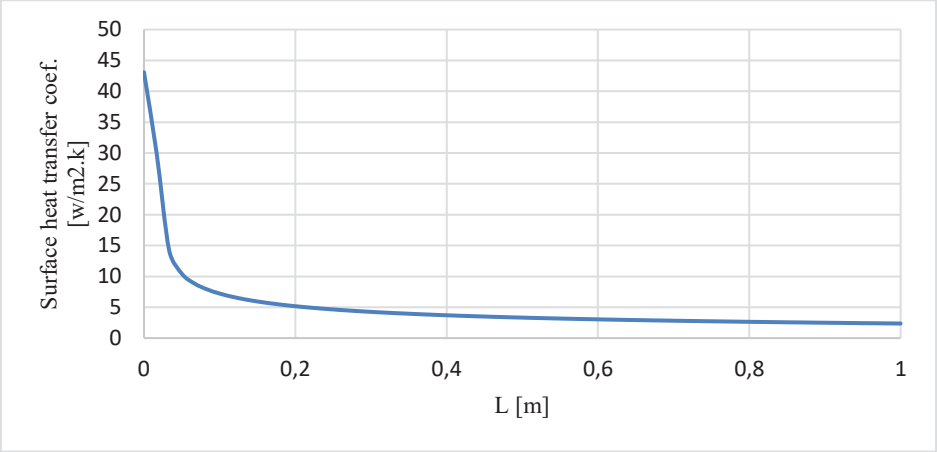


Figure 12. Surface heat transfer coefficient

5. VERIFICATION OF THE MODEL

The verification of the model has been done by comparing the CFD solution with the analytical solution of the average and local Nusselt number, average convection heat transfer coefficient, and the skin friction coefficient obtained via similarity technique [12] as the following:

5.1. Average Nusselt number ($\overline{Nu}_L$)

The comparison between the analytical and CFD for average Nusselt number ($\overline{Nu}_L$) shows good agreement and the error was only 2.896%. The result of the comparison presented in *Table 2* below:

Table 2

Result of ($\overline{Nu}_L$) CFD and analytical solution

Variable	Analytical	CFD	Error %
$\overline{Nu}_L$	192.820523	198.5766	2.896%

5.2. Local Nusselt number comparison (Nu_x)

The local Nusselt number can be calculated using the equation below:

$$Nu_x = \frac{q_x x}{(T_\infty - T_b)k}, \tag{16}$$

where:

q_x: heat flux at distance x,
x: distance from the leading edge,
T_∞: temperature of free stream,
T_b: bulk temperature of the fluid at x,
k: thermal conductivity of the fluid.

The local Nusselt number at different distances from the leading edge for the two solutions are shown in *Table 3*. The result shows a very good agreement between the two solutions. *Figure 13* shows the result of the comparison analytical and CFD solution of the local Nusselt number. The average error between the two solutions was 1.23%.

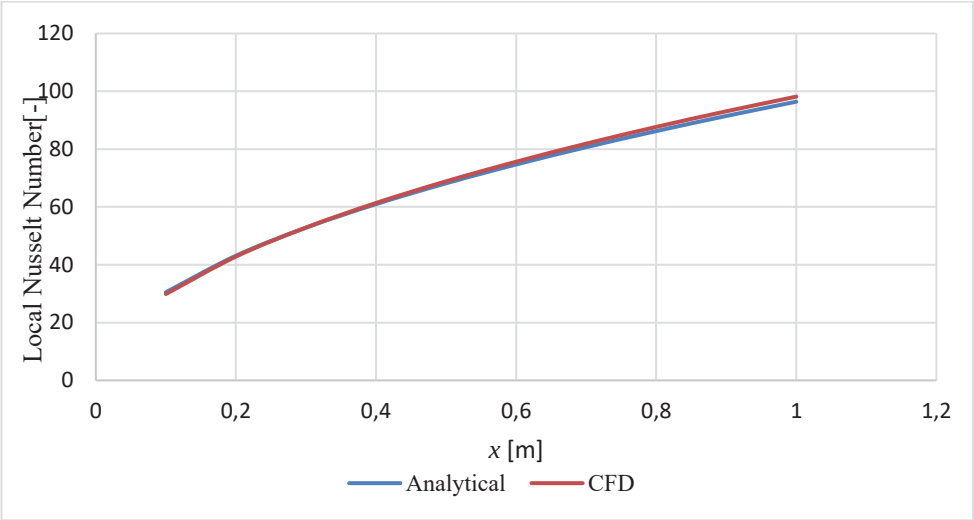


Figure 13. Comparison of analytical and CFD Results

Table 3
The result of local Nusselt Number

x	**Analytical**	**Fluent**	**Error%**
0.1	30.4876	29.8709	2.0645
0.2	43.1159	42.8180	0.6957
0.3	52.8060	52.8664	0.1141
0.4	60.9752	61.3597	0.6266
0.5	68.1723	68.8528	0.9882
0.6	74.6790	75.6342	1.2625
0.7	80.6626	81.8748	1.4795
0.8	86.2319	87.6792	1.6503
0.9	91.4628	93.0796	1.7363
1	96.4106	98.1585	1.7806

5.3. Average convection heat transfer ($\bar{h}$)

The results of $\bar{h}$, *Equation (8)* is presented in *Table 4* and it shows an excellent agreement between CFD and analytical solutions with only 0.0002% error.

Table 4
Result of comparison CFD and Analytical solutions

Variable	CFD	Analytical	Error %
$\bar{h}$	4.805554	4.66625	0.00002%

5.4. The skin friction coefficient

The skin friction using CFD is calculated by using the equation below:

$$C_f = \frac{0.664\tau_w}{\frac{1}{2}\rho\, v_b^2}, \tag{17}$$

where:
τ_w: wall shear stress at distance x from leading edge,
v_b: bulk velocity at distance x from leading edge,
C_f: skin friction coefficient,
ρ: density of the fluid.

A good agreement between CFD and the analytical solutions has been obtained. The results of the CFD and analytical solutions are represented in *Figure 14*. The average error between the two solutions is 6.19%. *Table 5* presents the results of the skin friction coefficient at a different distance from the leading edge. It shows that error is increasing with increasing value of *x*.

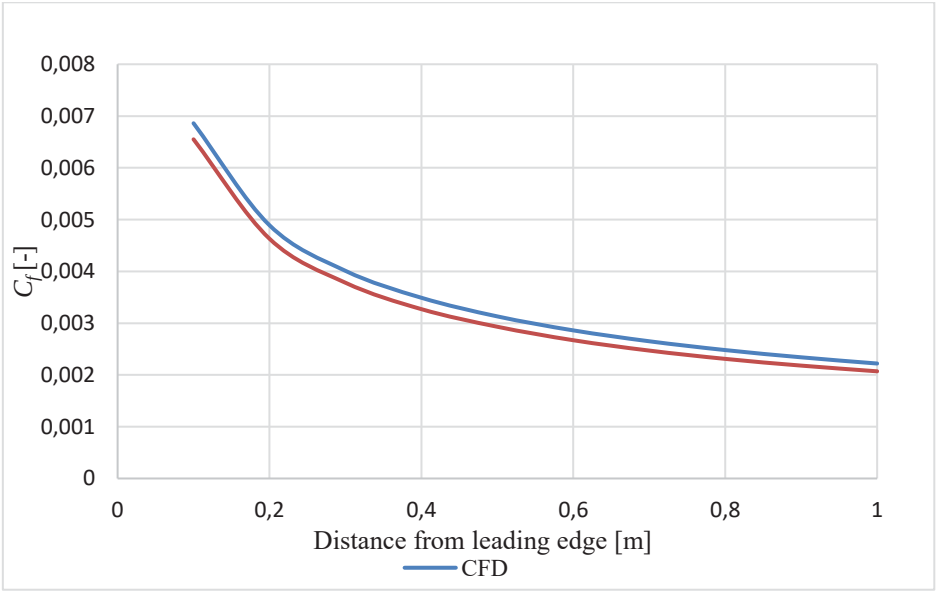


Figure 14. Comparison of the skin friction coefficients

Table 5
The skin friction coefficient

x	Analytical	CFD	Error%
0.1	0.00655	0.00686	4.49401
0.2	0.00463	0.00489	5.27362
0.3	0.00378	0.00401	5.78067
0.4	0.00327	0.00349	6.03457
0.5	0.00293	0.00313	6.37005
0.6	0.00267	0.00286	6.57521
0.7	0.00247	0.00265	6.74080
0.8	0.00231	0.00248	6.85560
0.9	0.00218	0.00234	6.87427
1	0.00207	0.00222	6.93961

6. ANALYZING THE EFFECT OF CHANGING THE LENGHT OF THE PLATE

Four simulations for different lengths from the leading edge was run for L = 0.8, 1, 1.2, and 1.4, with no change in the vertical dimension. All the model's properties in the model were fixed except the length of the horizontal dimensions. *Table 6* represents Reynolds' number for the four rectangles which were simulated for analysing the effect of changing the plate's length.

Table 6
Variation of the plate length

L	Re
0.8	82,150.44
1	102,688.05
1.2	123,225.66
1.4	143,763.27

6.1. The effect of the length on the velocity

The length of the plate effects on the velocity distribution and the boundary layer thickness. *Figure 15* shows the variation of the velocity at the outlet for different lengths. It is seen that the velocity decreases with the increment of the horizontal dimension and the boundary layer thickness gets higher values. The maximum value of the velocity was obtained for L = 0.8.

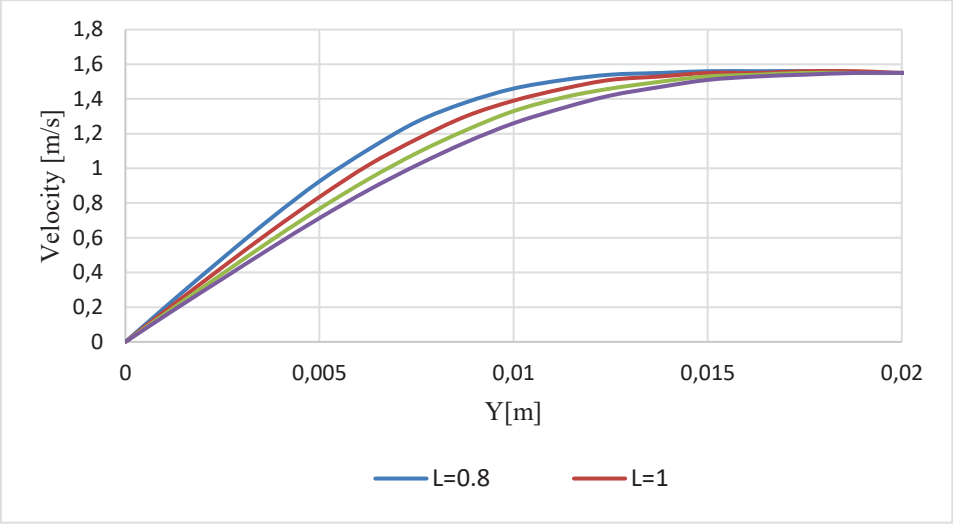


Figure 15. Velocity distribution and boundary layers for different plate's length

6.2. The effect of the plate length on the C_f, N_L, C_D, and τ_w

The skin friction coefficient plotted for the four length of the plate can be seen in *Figure 16* along with the length of the plate. At x = 0 the skin friction coefficient for L = 0.8 is 0.04517, for L = 1 is 0.04059, for L = 1.2 is 0.03715, and for L = 1.4 is 0.03446. The impact of the plate's length on the wall shear stress shown in *Figure 17* and *Table 7*, where the maximum value also was set as L = 0.8 and the wall shear stress is decreasing with increasing the plate's length. The comparison of the values of Nusselt number is plotted on *Figure 18*. It shows that the maximum value decreases with the increasing of the horizontal length. The conclusion is that the skin friction, wall shear stress and Nusselt number increase whenever the Reynolds number was increased. *Figure 19* demonstrates the variation of the drag coefficient with different plate lengths, it can be seen that the drag coefficient decreases as the plate length increases.

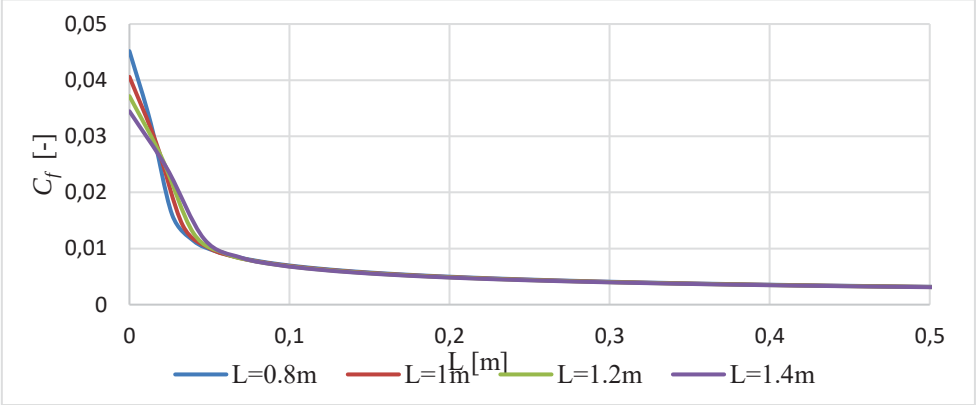


Figure 16. Skin friction coefficient for different plate's length

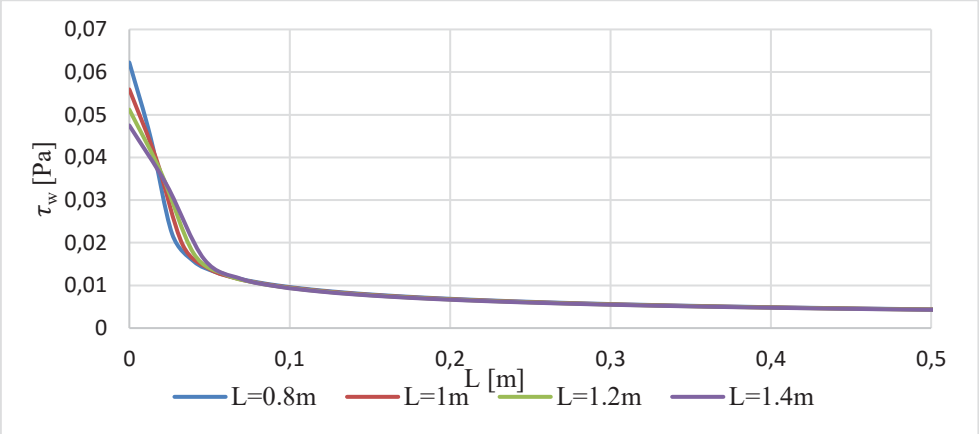


Figure 17. Wall shear stress for various L

Table 7
Wall shear stress at the leading edge

L	Wall shear
0.8	0.0622
1	0.0559
1.2	0.0512
1.4	0.0474

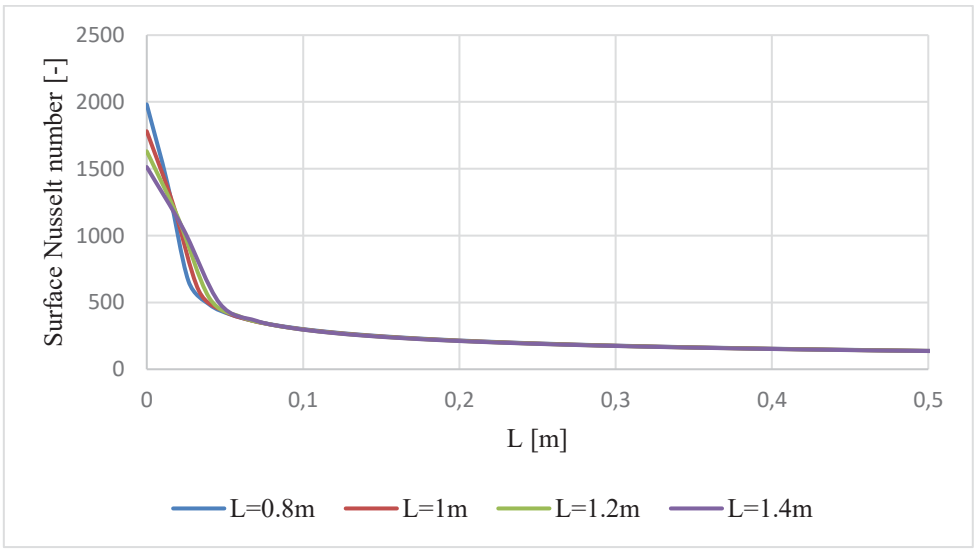


Figure 18. Nusselt number for different plate's lengths

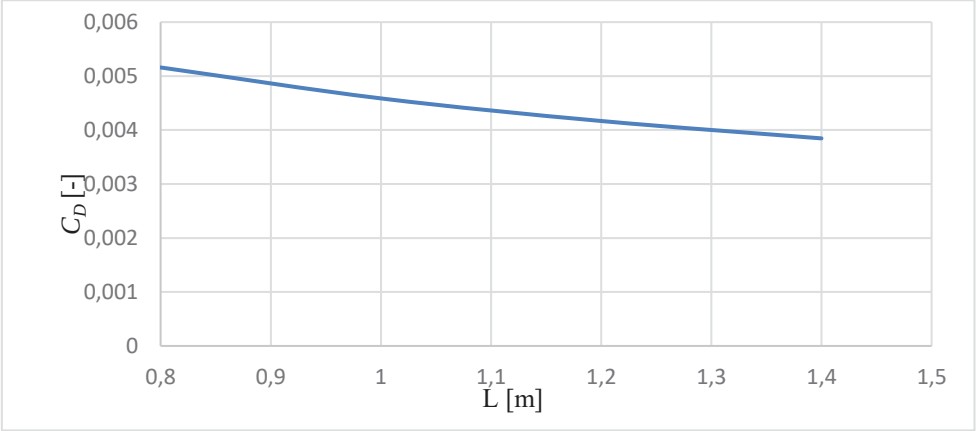


Figure 19. Drag coefficient for different plate's lengths

7. CONCLUSION

The hydrodynamic and thermal boundary layer of the air flow over a flat plate is numerically analysed using CFD simulation in two-dimensions. The results of the numerical and analytical solutions have been compared and showed good agreement for different variables in the model that have been simulated. Changing the length of the plate induced many effects on different dimensionless and dimensional variables such as Re, C_f, Nu, C_D, and the shear stress. Further study is recommended in the transition and turbulent flow for the same model.

NOMENCLATURE

C_f	–	skin frication coefficient
C_D	–	drag coefficient
F_x	N	horizontal force acting on the plate
$\bar{h}$	W/m^{2}k	average convection heat transfer
k	W/m.k	thermal conductivity of the fluid
N_{u_x}	–	local Nusselt number
$\overline{Nu}_L$	–	average Nusselt number
Pr	–	Prandtl number
q_x	W/m^2	heat flux at distance x
L	m	length of the plate
Re_x	–	Reynolds number at distance x
T_w	K	temperature of the plate
T_∞	K	temperature of free stream
T_b	K	bulk temperature of the fluid at x
u and v	m/s	components of the velocities
v_b	m/s	bulk velocity at distance x from leading edge

Greek symbols

υ	m^2/s	kinematic viscosity of the fluid
α	m^2/s	thermal diffusivity of the fluid

ρ	kg/m^3	density
μ	Pa/s	dynamic viscosity
τ_w	Pa	wall shear stress at distance *x* from leading edge.

Subscripts

w	wall
b	bulk

ACKNOWLEDGEMENT

The described study was carried out as part of the EFOP-3.6.1-16-2016-00011 *Younger and Renewing University – Innovative Knowledge City – institutional development of the University of Miskolc aiming at intelligent specialisation* project implemented in the framework of the Széchenyi 2020 program. The realization of this project is supported by the European Union, co-financed by the European Social Fund. The second author was supported by project no. 129257 implemented with the support provided from the National Research, Development and Innovation Fund of Hungary, financed under the K_18 funding scheme.

REFERENCES

[1] Blasius, H.: Grenzschichten in Flüssigkeiten mit kleiner Reibung. *Z. Math. Phys.,* 56 (1908), pp. 1–37.

[2] Howarth, L.: On the solution of the laminar boundary layer equations. *The Royal Soc. London*, A 164 (1938), pp. 547–579.

[3] Abu-Sitta, A. M. M.: A Note on a Certain Boundary-Layer. *Applied Mathematics and Computation*, 64 (1994), pp. 73–77.

[4] Zhang, J.–Chen, B.: An iterative method for solving the Falkner–Skan equation. *Appl. Math. Comput*., 210 (2009), pp. 215–222.

[5] Asaithambi, A.: Solution of the Falkner – Skan equation by recursive evaluation of Taylor coefficients. *Computational and Applied Mathematics*, 176 **(**2005), pp. 203–214.

[6] Bataller, R. C.: Numerical Comparisons of Blasius and Sakiadis Flows. *Matematika*, 26 **(**2010), pp. 187–196.

[7] Najafi, M.–Khoramishad, H.–Massah, H.–Moghimi, M.: A study of Blasius viscous flow : an ADM Analytical Solution. *Applied Mathematics*, 9 (2005), pp. 57–61.

[8] Wang, L.: A new algorithm for solving classical Blasius equation, *Applied Mathematics and Computation*, 157 **(**2004), pp. 1–9.

[9] Abbasbandy, S.: A numerical solution of Blasius equation by Adomian's decomposition method and comparison with homotopy perturbation method. *Chaos, Solitons and Fractals*, 31 (2007), pp. 257–260.

[10] Esmaeilpour, M.–Ganji, D. D.: Application of He's homotopy perturbation method to boundary layer flow and convection heat transfer over a flat plate. *Physics Letters*, A. 372 (2007), pp. 33–38.

[11] Ganji, D. D.–Babazadeh, H.–Noori, F.–Pirouz, M. M.–Janipour, M.: An Application of Homotopy Perturbation Method for Non-linear Blasius Equation to Boundary Layer Flow Over a Flat Plate Basic idea of homotopy perturbation method. *International Journal of Nonlinear Science*, 7 (2009), pp. 399–404.

[12] Schlichting, H.–Gersten, K.: *Boundary layer theory*. Springer Verlag, Berlin–Heidelberg–New York, 2000.